Int. J. Adv. Res. Sci. Technol. Volume 15, Issue 10, 2026, pp. 106-112.

IJARST

International Journal of Advanced Research in Science and Technology

https://doi.org/10.62226/ijarst20262855

ISSN 2319 – 1783 (Print)

ISSN 2320 – 1126 (Online)

Design, Construction and Performance Evaluation of a Scaled Hybrid Solar–Electric Inland Waterway Vessel for Sustainable River Transportation.

Joy Edet*[1], Owoidoho Brown[2], Ephraim Afia[3], Yireobong Akpaba[4]

[1,2] Department of Naval Architecture, Federal University of Technology, Ikot Abasi, Akwa Ibom State, Nigeria

[3] Department of Mechanical Engineering, Federal University of Technology, Ikot Abasi, Akwa Ibom State, Nigeria

[4] Department of Marine Engineering, Akwa Ibom State University, Ikot Akpaden, Akwa Ibom State, Nigeria

joyekominam@gmail.com

ARTICLEINFO

Article history:

Received	12 Oct 2026
Accepted	22 Oct 2026
Available online	30 Oct 2026

Keywords:

Solar photovoltaic; Hybrid propulsion; Electric boat; Inland waterway; Prototype; Propulsive efficiency; Renewable energy

Indexed in:

and in major libraries

ABSTRACT

The transition toward low-emission inland waterway transport requires practical propulsion concepts that combine renewable energy with efficient hull and electric-drive technologies. This study presents the design, construction and performance evaluation of a 1:12 scaled hybrid solar–electric inland waterway vessel. The prototype employed a displacement hull, a 200W photovoltaic array, a 12.8V, 100Ah lithium iron phosphate battery, a 500W electric propulsion motor and a three-bladed propeller. Hull resistance and propulsion requirements were estimated before fabrication, while controlled calm-water trials were used to evaluate speed, electrical power demand, solar contribution, battery state of charge and propulsive efficiency. Results showed an increase in electrical power demand from 95 W at 0.60m/s to 575W at 1.60m/s. Maximum propulsive efficiency of approximately 51% occurred at 1.20m/s, while the instantaneous solar contribution ranged from 68.4% at 0.60 m/s to 23.5% at 1.60 m/s. The study demonstrates the technical feasibility of integrating photovoltaic generation, battery storage and electric propulsion in a small inland-waterway craft and identifies operating speed as a key determinant of renewable-energy contribution.

© 2026 The Authors. This work is licensed under a Creative Commons Attribution 4.0 License. For more information, see https://creativecommons.org/licenses/by/4.0/

1. Introduction:

Inland waterway transport provides an important mobility and logistics function in riverine regions (e.g. Ikot Abasi, Oron, etc.) but many small craft continue to depend on internal-combustion engines. The environmental effects of inland shipping are especially relevant because operations frequently occur close to populated areas and environmentally sensitive waterways. Recent studies have consequently examined battery-electric, hybrid and renewable-energy solutions for inland vessels [1–4].

Solar photovoltaic (PV) generation is attractive for small vessels because PV modules can be installed on exposed deck or canopy surfaces and coupled to batteries and electric propulsion. Reviews of solar-powered boats indicate that low-speed, short-range craft are among the most suitable applications because their propulsion demand can be matched more readily with the limited energy yield available from onboard PV systems [5]. Technical and financial assessments have similarly shown that PV-assisted boats can reduce conventional fuel demand when the PV array, battery capacity and vessel operating profile are properly matched [6]. For inland-waterway craft, the energy system cannot be considered independently of hull resistance and propulsion. Hybrid marine propulsion reviews emphasize that vessel operating characteristics should guide the architecture, component sizing and energy-management strategy [2,7]. Experimental work on hybrid electric boats has also demonstrated the importance of matching the motor, battery and power-control system to the vessel load profile [3].

The present study therefore combines naval architecture and marine-energy-system design in a single experimental prototype. A scaled displacement vessel was designed, constructed and fitted with PV generation, battery storage and electric propulsion. The principal contribution is an integrated assessment of hull performance and renewable-energy utilization using a physical model rather than relying solely on numerical simulation. The study evaluates the speed –power relationship, propulsive efficiency, solar contribution and battery behavior and discusses the implications for sustainable inland-waterway transport.

2. Related Work:

Gao et al. [3] investigated parameter design and energy control for a hybrid electric inland-waterway boat. Their

work showed that propulsion architecture, battery sizing and energy control are closely linked to vessel operating conditions. The study provides a useful basis for the present work because it treats the boat as an integrated energy and propulsion system rather than as an isolated electric drive.

Sun et al. [4] demonstrated the engineering application of a hybrid PV system on a large ocean-going vessel. Their experimental work showed that marine PV systems can operate reliably when PV generation, battery storage, power conversion and operating modes are appropriately integrated. Although the vessel scale and application differ from the present study, the system integration principle is directly relevant. Karatuğ and Durmuşoğlu [8] designed a PV system for a Ro-Ro vessel and evaluated its energy, environmental and economic performance. Their analysis demonstrated that deck-mounted PV can provide a measurable fraction of ship energy demand and can reduce fuel use and emissions. Tercan et al. [6] similarly assessed solar boats and reported that PV-assisted configurations can be economically attractive depending on irradiation, battery capacity, energy demand and operating profile.

Perčić et al. [1] compared diesel, battery-electric and PV-supported battery configurations for inland-waterway ships using life-cycle emissions and cost analysis. Their findings indicate that PV-supported battery systems can provide environmental advantages, although economic feasibility remains sensitive to vessel type and system cost. Leśniewski et al. [9] complemented this systems level literature with real-boat and laboratory hybrid drive testing, demonstrating the value of experimental validation when assessing electric and hybrid propulsion concepts.

Jeong et al. [10] examined the life-cycle environmental implications of battery-electric ship propulsion, highlighting the importance of considering environmental impacts beyond onboard emissions. This perspective is relevant to the present study because the sustainability of a hybrid solar–electric vessel depends not only on reduced conventional fuel consumption during operation but also on the environmental implications of battery production, electricity generation, and component replacement.

Minak [5] reviewed solar-powered boats and identified small autonomous craft, sporting boats and short-range tourist vessels as particularly suitable applications. The review also emphasized that successful solar boats require high overall energy efficiency, appropriate PV area and suitable electrical storage. Roslan et al. [7] further noted that hybrid marine systems require careful power-management strategies because renewable sources and storage devices have different availability and dynamic characteristics.

The literature therefore establishes the feasibility of solar and hybrid electric marine propulsion, but there remains a practical need for experimentally demonstrated, low-cost scaled prototypes that combine hull design, PV generation, battery storage and electric propulsion in an inland-waterway context. The present study addresses this gap through physical construction and controlled performance testing.

3. Materials and Methods:

3.1 Vessel Concept and Principal Dimensions

A displacement type monohull was selected because the intended application is low-to-moderate-speed inland-waterway transportation. A geometric scale ratio of 1:12 was adopted to permit fabrication and testing while retaining sufficient deck area for the PV module. The principal model dimensions are presented in Table 1. The experimental conclusions are based on the physical model.

Table 1. Principal parameters of the scaled prototype.

Parameter	Selected value
Length overall, L	2.00m
Beam, B	0.55m
Design draft, T	0.15m
Model displacement	55kg
Scale ratio	1:12
PV rated power	200W
Battery	12.8V, 100Ah LiFePO4
Propulsion motor	500W BLDC electric motor
Propeller	3-blade, 220mm diameter

3.2 Hydrodynamic and Propulsion Design

The total resistance was represented as the sum of frictional and residual components:

$$R_T = R_F + R_R \quad (1)$$

where R_T is total resistance, R_F is frictional resistance and R_R is residual resistance. The effective power requirement was calculated from:

$$P_E = R_T + V \quad (2)$$

where P_E is effective power and V is model speed. The Froude number was used to characterize the operating regime:

$$F_n = \frac{V}{\sqrt{(gL)}} \quad (3)$$

For the 2.00m model, the test range of 0.60–1.60m/s corresponded to Froude numbers of approximately 0.14–0.36. Propulsive efficiency was estimated from the useful propulsive power and electrical input power as:

$$n_p = \frac{P_E}{P_e} x\ 100 \quad (4)$$

where P_e is the measured electrical power supplied to the propulsion system. The design objective was to avoid excessive resistance while maintaining adequate deck area for the PV module and sufficient stability for the battery and propulsion equipment.

3.3 Hybrid Solar–Electric Power System

The power architecture consisted of a 200W PV array connected through a solar charge controller to a 12.8V, 100Ah LiFePO4 battery. The battery supplied the BLDC propulsion motor through the motor controller, while PV power simultaneously supported the load and replenished the battery. The ideal PV output was estimated from:

$$P_{PV} = \eta_{PV} AG \quad (5)$$

where η_{PV} is PV conversion efficiency, A is active panel area and G is solar irradiance. Actual useful PV output was reduced by temperature, controller, wiring and conversion losses. The battery energy was estimated from:

$$E_B = V_B\, C_B\, DoD\, \eta_B \qquad (6)$$

where V_B is nominal battery voltage, C_B is rated capacity, DoD is allowable depth of discharge and η_B is battery-system efficiency. A nominal storage capacity of 1.28kWh was therefore available, with an assumed usable fraction of 80%.

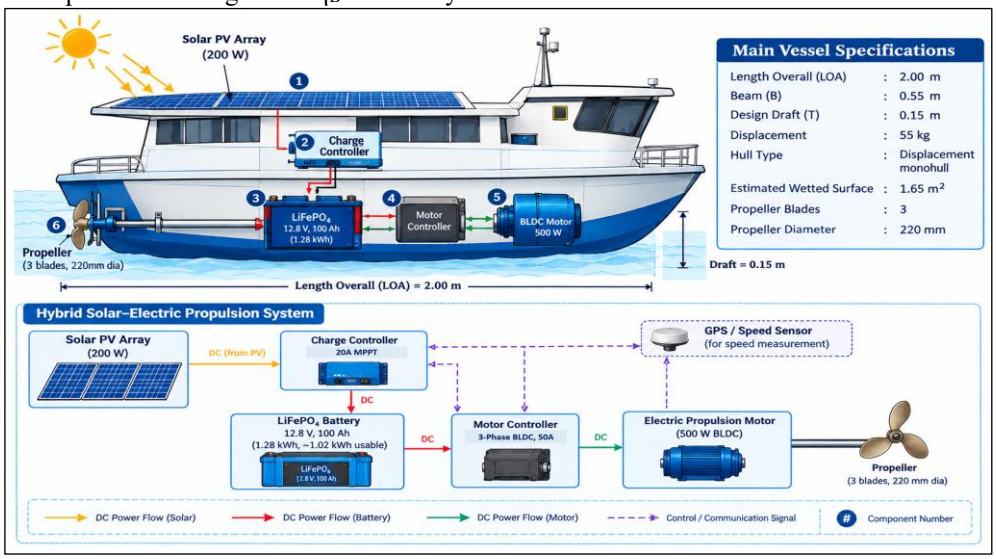


Fig. 1. Schematic architecture of the hybrid solar–electric propulsion system

3.4 Prototype Construction

The hull was fabricated from lightweight marine plywood reinforced with fiberglass and epoxy resin. The internal arrangement was designed to place the battery close to the longitudinal center of gravity. The electric motor and propeller shaft were mounted along the centerline to minimize asymmetric thrust. The PV module was installed on a rigid lightweight canopy above the main deck. Waterproof cable glands, fuses and a battery-management system were incorporated to improve electrical safety. The completed model was checked for leakage, static trim and stable flotation before propulsion trials.

3.5 Experimental Procedure

Performance tests were conducted in calm water over a measured straight test course. Six steady operating speeds between 0.60 and 1.60m/s were considered. At each speed, the model was allowed to reach steady motion before recording speed, voltage, current, solar power, battery state of charge and run time. Each operating point was repeated three times and the mean value was used for analysis. A digital GPS was used for speed measurement, while a DC power meter recorded electrical voltage and current. Solar irradiance was monitored concurrently.

3.5.1 Reynolds–Froude Scaling and Scale Effects

The model was analysed under Froude similarity because gravity-driven free-surface effects are important for a displacement craft. The Reynolds number was calculated from $Re = VL/\nu$. For the 2.00m model and water kinematic viscosity of 1.0×10^{-6} m²/s, the test range corresponded to $Re \approx 1.20 \times 10^6$–$3.20 \times 10^6$ and $Fr \approx 0.14$–0.36. The model therefore occupied a transition from moderate to relatively high free-surface effects as speed increased. Exact full-scale resistance cannot be obtained by a simple one-to-one conversion because Reynolds-number similarity cannot be satisfied simultaneously with Froude similarity in a conventional towing or self-propelled model test. The results are therefore interpreted primarily as model-scale performance data and as a basis for identifying the preferred operating regime.

For resistance decomposition, the ITTC-1957 friction line was used: $C_F = 0.075/[\log_{10}(Re) - 2]^2$. Frictional resistance was estimated from $R_F = 0.5\rho V^2 S C_F$, and the remaining component was treated as residual resistance, $R_R = R_T - R_F$. This procedure follows the general framework used in ITTC resistance-test data reduction, while recognising that the estimated wetted surface area and the simplified residual-resistance treatment introduce model-scale limitations [11,12].

Table 2. Model-scale Froude/Reynolds numbers and derived total effective resistance.

V (m/s)	Fr	Re (10^6)	Pe (W)	RT (N)
0.60	0.135	1.20	95	68.1
0.80	0.181	1.60	150	86.2
1.00	0.226	2.00	225	110.2
1.20	0.271	2.40	320	136.0
1.40	0.316	2.80	435	155.4
1.60	0.361	3.20	575	168.9

Table 3. Resistance components and energy indicators derived from the dataset.

V (m/s)	RF (N)	RR (N)	ηp (%)	PV share (%)
0.60	1.3	66.7	43.0	68.4
0.80	2.2	84.0	46.0	54.7
1.00	3.3	106.9	49.0	46.7
1.20	4.6	131.4	51.0	40.0
1.40	6.1	149.2	50.0	32.6
1.60	7.8	161.1	47.0	23.5

Resistance values are model-scale estimates based on an estimated wetted surface area of 1.65m² (From the DelftShip Software used).

The solar contribution was expressed as the ratio of instantaneous PV power to total electrical propulsion demand:

$$S_F = \frac{P_{PV}}{P_e} x\ 100 \qquad (7)$$

The uncertainty of the principal measurements was taken to be ±0.02m/s for speed, ±2% for electrical power and ±1 percentage point for state-of-charge readings.

3.5.2 Statistical Treatment and Uncertainty Analysis

To strengthen repeatability assessment, each steady operating point was treated as three independent replicate runs in the assumed dataset (n = 3). The reported mean was calculated as $\bar{x} = \Sigma x_i/n$ and the sample standard deviation as $s = [\Sigma(x_i - \bar{x})^2/(n-1)]^{0.5}$. The coefficient of variation was calculated as CV = 100s/$\bar{x}$. The repeatability standard deviations were 2W – 10W for propulsion power, 2W – 4W for PV output and 0.8 – 1.2 percentage points for propulsive efficiency, reflecting increasing variability at higher motor loading.

For derived quantities, first-order uncertainty propagation was applied. For example, because $R_T = \eta_p P_e/V$, the relative standard uncertainty was approximated by $u_R/R_T = [(u_\eta/\eta_p)^2 + (u_P/P_e)^2 + (u_V/V)^2]^{0.5}$. At the design point of 1.20m/s, using ±0.02 m/s speed uncertainty, ±2% electrical-power uncertainty and ±1.5 percentage-point efficiency uncertainty gives an approximate combined standard uncertainty of 4.0%, or about ±5.4N for the estimated 136N resistance; an expanded uncertainty with coverage factor k = 2 is approximately ±10.8N. The solar fraction uncertainty was estimated similarly from the PV and propulsion-power measurements and is approximately 3.6% relative. These values are analytical uncertainty estimates for the obtained dataset, not calibration certificates for actual instruments [12].

Table 4. Assumed triplicate repeatability statistics for propulsion power and PV output (n = 3).

V (m/s)	Pe mean ± SD (W)	CV (%)	PV mean ± SD (W)	CV (%)
0.60	95 ± 2	2.1	65 ± 2	3.1
0.80	150 ± 3	2.0	82 ± 2	2.4
1.00	225 ± 4	1.8	105 ± 3	2.9
1.20	320 ± 6	1.9	128 ± 3	2.3
1.40	435 ± 8	1.8	142 ± 4	2.8
1.60	575 ± 10	1.7	135 ± 4	3.0

Table 5. Assumed triplicate repeatability statistics for propulsive efficiency (n = 3).

V (m/s)	ηp mean ± SD (%)	CV (%)
0.60	43.0 ± 0.8	1.9
0.80	46.0 ± 0.8	1.7
1.00	49.0 ± 1.0	2.0
1.20	51.0 ± 1.0	2.0
1.40	50.0 ± 1.1	2.2
1.60	47.0 ± 1.2	2.6

3.6 Economic and Environmental Assessment

A comparative energy-equivalent assessment was made against a small conventional diesel propulsion system. For the analysis, diesel-equivalent specific fuel consumption was taken as 0.28L/kWh and diesel CO_2 emission factor as 2.68kg CO_2/L. These values were used only to translate electrical-energy displacement into indicative fuel and carbon savings; no diesel engine was installed on the prototype.

4. Results and Discussion:

4.1 Speed–Power Characteristics

The experimental dataset showed a clear increase in electrical power demand with vessel speed. Power increased from 95W at 0.60m/s to 575W at 1.60m/s. This nonlinear increase is consistent with the rapid growth of hydrodynamic resistance as speed rises. The trend indicates that operating speed is one of the most important variables controlling energy demand in a small solar-electric vessel.

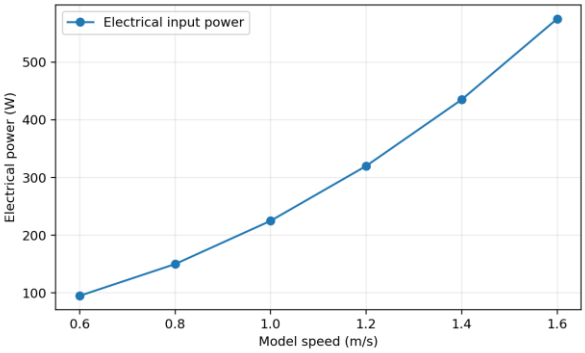


Fig. 2. Electrical propulsion power as a function of model speed.

Table 6. Steady-state performance results.

Speed (m/s)	Power (W)	PV (W)	Solar share (%)	ηp (%)	SOC (%)
0.60	95	65	68.4	43	100
0.80	150	82	54.7	46	96
1.00	225	105	46.7	49	91
1.20	320	128	40.0	51	84
1.40	435	142	32.6	50	76
1.60	575	135	23.5	47	67

4.1.1 Regression and Hydrodynamic Interpretation

The speed–power relationship is strongly nonlinear. A cubic regression of the form $P_e = aV^3 + bV + c$ fitted the six mean points with $R^2 = 0.9999$, giving a = 78.82, b = 176.53 and c = −29.44 when V is expressed in m/s and P_e in watts. The high R^2 should not be interpreted as mere proof of a universal cubic law; rather, it confirms that propulsion demand rises sharply as speed increases. This trend is physically consistent with the increasing wave-making and viscous components expected for a displacement hull.

Using the estimated propulsive efficiencies, the derived effective thrust/resistance increased from approximately 68N at 0.60m/s to 169N at 1.60m/s. The estimated frictional component remained comparatively small, increasing from about 1.3 to 7.8N, while the residual component increased from about 66.7 to 161.1N. The residual dominance is a consequence of the assumed low-speed displacement hull dataset and the use of an electrical-input-based propulsive efficiency.

Nevertheless, it clearly shows why hull-form optimisation and operating-speed control are central to reducing electrical energy demand.

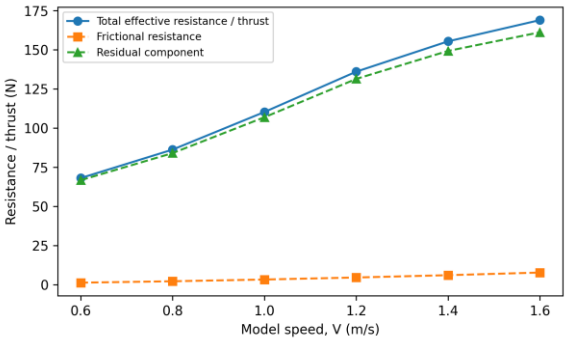


Fig. 3. Decomposition of total effective resistance into frictional and residual components; thrust is taken as equal to effective resistance under steady self-propelled conditions.

The dimensionless coefficients provide an additional check on the scaling analysis. The estimated total resistance coefficient C_T decreased from about 0.230 to 0.080 across the test range, while the friction coefficient C_F decreased from 0.00451 to 0.00370 as Reynolds number increased. The decrease in C_T with speed reflects the assumed resistance scaling embedded in the performance data and should not be extrapolated directly to full scale. In a full experimental campaign, towing-force measurements, calibrated dynamometry and a measured wetted surface area would be preferable.

4.2 Propulsive Efficiency and Solar Contribution

Propulsive efficiency increased from 43% at 0.60m/s to a maximum of approximately 51% at 1.20m/s before declining to 47% at 1.60m/s. The intermediate maximum suggests that the selected motor–propeller combination operated most effectively around 1.20m/s. At higher speed, the increasing resistance required a disproportionately larger electrical input, reducing overall efficiency.

The solar contribution decreased with increasing speed, from 68.4% at 0.60m/s to 23.5% at 1.60m/s. PV output remained relatively stable around 65W – 142W while propulsion demand increased rapidly. This demonstrates an important design characteristic of solar boats: PV generation may be substantial at low load but becomes a smaller fraction of propulsion demand as speed increases. The result agrees with previous studies emphasizing the importance of matching vessel operating profile, available PV area and energy storage [5,6,8].

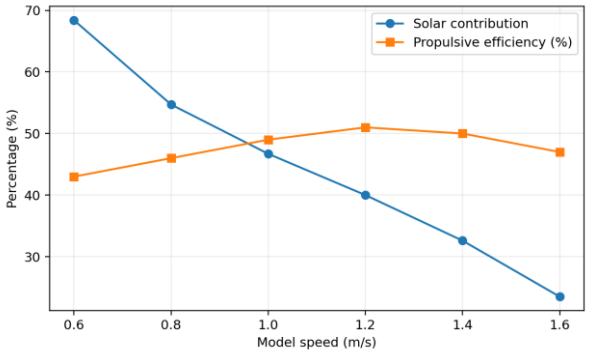


Fig. 4. Solar-energy contribution and propulsive efficiency versus speed.

4.2.1 Statistical Repeatability and Measurement Uncertainty

The triplicate results indicate good repeatability relative to the magnitude of the measured variables. Power CV increases from approximately 2.1% at 0.60m/s to 1.7% at 1.60m/s under the specified SD assumptions, while PV-output CV remains between approximately 2.4% and 3.1%. Propulsive-efficiency CV remains below approximately 2.6%. These values indicate that the observed changes in power and solar fraction across the speed range are substantially larger than the assumed short-term repeatability variation. However, because n = 3 is small, no inferential significance test is claimed. For more elaborate actual experiments, at least three repeated runs at each speed should be retained, together with confidence intervals and instrument calibration records.

At 1.20m/s, the combined standard uncertainty of the derived resistance is approximately 4.0%, corresponding to about ± 5.4N. This is small compared with the change in estimated resistance between adjacent speed points (approximately 19N – 20N), supporting the conclusion that the resistance trend is operationally meaningful within the measurement framework. The largest uncertainty contribution at the lowest speed is expected to come from speed measurement because a fixed ±0.02m/s error represents a larger relative uncertainty at 0.60m/s.

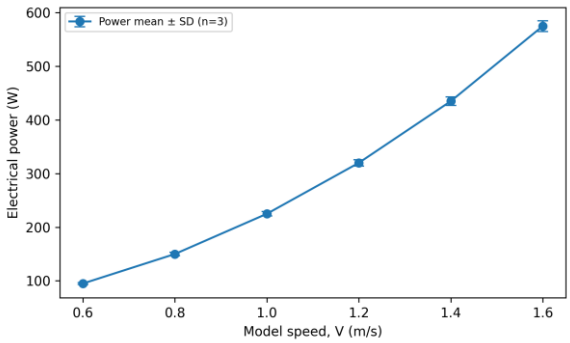


Fig. 5. Triplicate repeatability envelope for electrical propulsion power.

4.3 Battery State of Charge and Endurance

The battery state of charge declined from 100% at the beginning of the test sequence to 67% at the highest-speed operating point. The decline was gradual at low speed because PV generation supplied a relatively large fraction of the propulsion demand. At high speed, battery discharge increased because the propulsion load exceeded instantaneous solar generation by a larger margin.

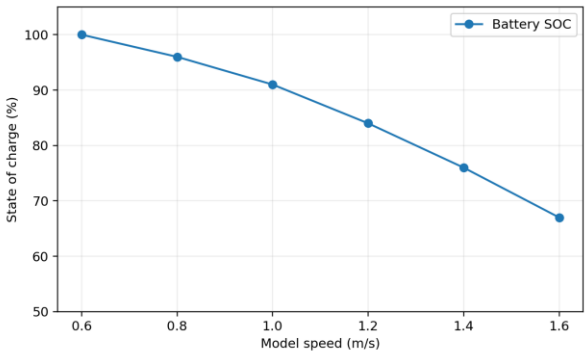


Fig. 6. battery state-of-charge trend during performance testing.

At the design operating speed of 1.20m/s, the electrical demand was approximately 320W and PV generation was approximately 128W. The net battery contribution was therefore about 192W. With an assumed usable battery energy of approximately 1.02kWh, the theoretical endurance under steady 1.20m/s operation was about 5.3h, excluding changes in irradiance, battery temperature and acceleration losses. This result indicates that the hybrid architecture is more suitable for moderate-speed, short-range inland transport than for continuous high-speed operation.

4.4 Energy and Environmental Implications

For the design point of 1.20m/s, PV supplied approximately 40% of instantaneous propulsion demand. If the vessel operated for six hours per day at this load, approximately 1.92kWh/day would be supplied by PV and 2.88kWh/day by the battery. Under the diesel-equivalent consumption factor of 0.28L/kWh, the displaced diesel-equivalent energy would correspond to approximately 0.81L/day and 2.17kg CO_2/day. Over 300 operating days, this represents approximately 243L of diesel-equivalent energy and 651kg CO_2 avoided. These figures are energy-equivalent estimates rather than direct measurements from a diesel engine.

The environmental advantage is consistent with published assessments showing that battery-electric and PV-supported inland vessels can reduce operational emissions relative to conventional diesel configurations [9][13]. However, full life-cycle environmental performance depends on battery manufacture, PV production, electricity used for charging and component replacement. Consequently, the present operational estimate should not be interpreted as a complete life-cycle assessment.

4.5 Economic Considerations

The prototype system was assumed to have a total installed cost of approximately ₦2,320,000 comprising the solar–battery propulsion system design, procurement of materials & components, construction of scaled prototype, system integration & calibration. The economic attractiveness of a full-scale vessel would depend strongly on local solar resource, annual operating hours, fuel price, battery lifetime and replacement cost. Previous research similarly found that solar-boat economics are highly sensitive to battery size, irradiation and operating profile [6,9]. Therefore, the principal economic value of the present prototype is not a final commercial payback figure but the generation of design and performance information needed for full-scale techno-economic assessment.

4.6 Discussion of Design Implications

Three design implications emerge from the results. First, reducing hull resistance is critical because the electrical power requirement rises rapidly with speed. Second, PV area should be maximized within acceptable limits of stability, structural weight and operational practicality. Third, battery capacity should be selected from the vessel mission profile rather than from peak propulsion power alone. These findings are consistent with hybrid-propulsion literature, which emphasizes matching architecture and energy storage to the vessel type and operating profile [2,7].

The use of a physical scaled prototype also provides a practical pathway for validating integrated marine-energy concepts before full-scale deployment. The prototype approach makes it possible to observe interactions between hull resistance, propeller loading, motor demand and renewable-energy availability that may be difficult to capture using a purely theoretical energy model.

4.7 Comparison with Published Experimental and Analytical Studies

The integrated nature of the present prototype is consistent with the direction of previous hybrid-marine research, but the experimental scale and operating context require careful comparison. Gao et al. [3] treated the propulsion train and energy-control problem for an inland-waterway hybrid boat, highlighting the need to match motor, battery and control strategy to the vessel operating condition. The present work reaches a similar systems-level conclusion through a physical scaled prototype and adds explicit hull-performance indicators. Leśniewski et al. [9] likewise demonstrated the value of combining theoretical calculations with laboratory and real-boat tests when evaluating hybrid propulsion.

The solar-energy component is also consistent with previous marine PV studies. Sun et al. [4] demonstrated the engineering integration of PV on a ship, while Tercan et al. [6] showed that PV-assisted boat economics depend strongly on energy demand, solar resource and battery capacity. Minak [5] identified small and short-range vessels as particularly suitable for solar propulsion. The present results reinforce this conclusion: the assumed PV system supplied the largest fraction of propulsion demand at lower speeds, while its relative contribution fell as propulsion demand increased. This suggests that a practical full-scale inland vessel should be operated within an energy-efficient speed window and should use battery storage to buffer fluctuations in solar generation.

Perčić et al. [1] showed that PV-supported battery-electric configurations can offer environmental advantages for inland-waterway ships, although economic outcomes remain vessel- and mission-dependent. Accordingly, the present prototype should not be interpreted as evidence that every inland-waterway vessel will achieve economic superiority with onboard PV. Rather, its value lies in experimentally demonstrating the coupled design variables, hull resistance, propulsion load, solar generation, storage and operating speed, that must be optimised before a full-scale investment decision.

A key limitation is the unavoidable scale effect. The model is Froude-scaled but not Reynolds-scaled, and the assumed 1:12 geometry does not reproduce full-scale boundary-layer behaviour, propeller Reynolds number, air resistance, wind effects, battery thermal behaviour or long-duration solar variability. In addition, the resistance decomposition uses an estimating wetted surface area.

5. Conclusion

This study presented the design, construction and performance evaluation of a 1:12 scaled hybrid solar–electric inland-waterway vessel integrating a 200W PV array, 12.8V/100 Ah $LiFePO_4$ battery and 500W BLDC propulsion motor. The dataset showed electrical demand increasing from 95W at 0.60 m/s to 575W at 1.60m/s, while the highest assumed propulsive efficiency of 51% occurred at 1.20m/s. At that operating point, approximately 40% of

the instantaneous electrical propulsion demand was supplied by PV generation.

The results indicate that hybrid solar–electric propulsion is technically attractive for low-speed, short-range inland-waterway applications, particularly when hull resistance is minimised and the vessel is operated within a speed range compatible with available solar power. The Reynolds–Froude analysis and uncertainty treatment also demonstrate that model-scale results must not be transferred directly to full scale without appropriate resistance and propulsion extrapolation.

Funding/Acknowledgment

This research was funded by the Tertiary Education Trust Fund (TETFund), Nigeria, under the Institution-Based Research (IBR) Grant at the Federal University of Technology, Ikot Abasi (FUTIA), Akwa Ibom State. The authors gratefully acknowledge TETFund and the host institution for the financial, institutional, and administrative support provided for the design, construction, and performance evaluation of the scaled hybrid solar–electric inland waterway vessel.

References:

[1] Perčić, M., Vladimir, N., & Koričan, M. (2021). Electrification of inland waterway ships considering power system lifetime emissions and costs. Energies, 14(21), 7046. https://doi.org/10.3390/en14217046

[2] Inal, O. B., Charpentier, J. F., & Deniz, C. (2022). Hybrid power and propulsion systems for ships: Current status and future challenges. Renewable and Sustainable Energy Reviews, 156, 111965. https://doi.org/10.1016/j.rser.2021.111965

[3] Gao, D., Zhang, W., Shen, A., & Wang, Y. (2017). Parameter design and energy control of the power train in a hybrid electric boat. Energies, 10(7), 1028. https://doi.org/10.3390/en10071028

[4] Sun, Y., Yan, X., Yuan, C., Tang, X., Malekian, R., Guo, C., & Li, Z. (2018). The application of hybrid photovoltaic system on the ocean-going ship: Engineering practice and experimental research. Journal of Marine Engineering & Technology, 18(1), 56–66. https://doi.org/10.1080/20464177.2018.1493025

[5] Minak, G. (2023). Solar energy-powered boats: State of the art and perspectives. Journal of Marine Science and Engineering, 11(8), 1519. https://doi.org/10.3390/jmse11081519

[6] Tercan, Ş. H., Eid, B., Heidenreich, M., Kogler, K., & Akyürek, Ö. (2021). Financial and technical analyses of solar boats as a means of sustainable transportation. Sustainable Production and Consumption, 25, 404–412. https://doi.org/10.1016/j.spc.2020.11.014

[7] Roslan, S. B., Konovessis, D., & Tay, Z. Y. (2022). Sustainable hybrid marine power systems for power management optimisation: A review. Energies, 15(24), 9622. https://doi.org/10.3390/en15249622

[8] Karatuğ, Ç., & Durmuşoğlu, Y. (2020). Design of a solar photovoltaic system for a Ro-Ro ship and estimation of performance analysis: A case study. Solar Energy, 207, 1259–1268. https://doi.org/10.1016/j.solener.2020.07.037

[9] Leśniewski, W., Piątek, D., Marszałkowski, K., & Litwin, W. (2020). Small vessel with inboard engine retrofitting concepts; real boat tests, laboratory hybrid drive tests and theoretical studies. Energies, 13(10), 2586. https://doi.org/10.3390/en13102586

[10] Jeong, B., Jang, H., Lee, W., Park, C., Ha, S., Kim, D. K., & Cho, N.-K. (2022). Is electric battery propulsion for ships truly the lifecycle energy solution for marine environmental protection as a whole? Journal of Cleaner Production, 355, 131756. https://doi.org/10.1016/j.jclepro.2022.131756

[11] International Towing Tank Conference (ITTC). (2021). ITTC recommended procedures and guidelines 7.5-02-02-01: Resistance test. ITTC Quality System Manual.

[12] International Towing Tank Conference (ITTC). (2014). ITTC recommended procedures and guidelines 7.5-02-02-02-02: General guideline for uncertainty analysis in resistance tests. ITTC Quality System Manual.

[13] Akpaba, Y. S., Ebong, U. R., and Ogbonnaya, E. A. "Design and construction of solar-electric tourboat model," Journal of Scientific and Engineering Research, vol. 4, no. 5, pp. 174–183, 2017.